Technical Design Report

April 24th, 2022

Team Member	Role	Department
Alex D. Santiago Vargas	Lead	Electrical Engineering
Idalina L. Claudio Rodríguez	Sub-Lead	Mechanical Engineering
Gadiel J. Matheu Vega	Mechanical Design	Mechanical Engineering
José A. Pedraza Centeno	Generator Design	Electrical Engineering
Gabriel A. Vera Rodríguez	Controls and Power System	Electrical Engineering
Alcides Ramos	Structural	Civil Engineering
Ariel Torres Rivera	Structural	Mechanical Engineering
Dr. Amaury Malave Sanabria	Faculty Advisor	Mechanical Engineering
Dr. Diego A. Aponte Roa	Supporting Faculty	Electrical Engineering
Dr. Rolando García González	Supporting Faculty	Civil Engineering
Dr. Albert Espinoza	Supporting Faculty	Mechanical Engineering
José Santana	Supporting Faculty–Machinist	Mechanical Engineering

Sponsors

Table of Contents

Table of Contents ..... b
List of Figures c
List of Tables c
Executive Summary ..... d
1. Introduction 1
2. Structural Design 1
2.1. Foundations Structural Analysis 1
2.2. Foundations Prototype Testing 2
3. Electrical Design 5
3.1. Generator Design 5
3.2. Electric Brake Testing 6
3.3. Generator Testing 7
3.4. Control Circuit 8
3.5. Voltage and Current Sensor Filters Testing 10
4. Mechanical Design 11
4.1. Blades 11
4.2. Hub 12
4.3. Generator 13
4.4. Nacelle, Turntable, and Tail 14
5. Turbine Assembly Checklist 16
6. Conclusion 17
7. References i

List of Figures

Figure 1. Forces applied to piles 1
Figure 2. Foundation Tripod Assembly and Single Pile Below 3
Figure 3. Single pile at maximum resistance and after breaking loose 3
Figure 4. Reduction of 3D AFPM FEM Analysis to 2D FEM. Taken from [2] 5
Figure 5. AFPM Generator Magnetic Finite Element Analysis with MATLAB/FEMM 6
Figure 6. AFPM Generator Magnetic Field Density Across Coils 6
Figure 7. Electric Brake 7
Figure 8. Electric Brake Test Set-Up 7
Figure 9. Generator Final Assembly 8
Figure 10. Open Circuit Generator Induced Voltage at 1,300 RPM 8
Figure 11. Block Diagram 9
Figure 12. Control Circuit Box 9
Figure 13. Control Logic Loop 10
Figure 14. Pass Band Gain 10
Figure 15. Cut-Off Frequency Gain 11
Figure 16. Stop Band Gain 11
Figure 17. Blades Coefficient of Power Curve 12
Figure 18. Hub Features (Back on the left, Front on the right). 13
Figure 19. Generator CAD Model 14
Figure 20. Generator Stator Assembly 14
Figure 21. Nacelle Exploded View 15
Figure 22. Air Flow Simulation on the Nacelle 15
Figure 23. Turbine Assembly 16
Figure 24. Turbine Exploded View 17

List of Tables

Table 1. Node reactions 2
Table 2. Resistance test results 4
Table 3. Turbine Components from Exploded View 17

Executive Summary

Juracan Energy Team is a group of students founded for the 2016 Collegiate Wind Competition (CWC) in Universidad del Turabo, now known as Universidad Ana G. Mendez. Through the years the team took part in the 2016 CWC, 2017 CWC, and 2019 CWC as well as the 2020 Marine Energy Collegiate Competition (MECC). The team won one resiliency award, two people choice and one bonus challenge awards in the CWC and the third place overall at the MECC. This year the team is taking part as a learn-along team in the 2022 CWC and in the 2022 Solar District Cup.

The name Juracan is derived from the female Taino deity Juracan who was once believed to be goddess lady of the winds, storm, and destruction. Juracan Energy Team represents the hardships from being and island community and how we seek energy stability through storms and destruction we island communities are exposed to.

This report is the result of the 2022 team developing for the first time an offshore micro wind turbine. Under the mentorship of Dr. Amaury Malavé we improved on the 2019 design by strengthening the hub, improving the blades, and creating a detailed methodology to design the generator from scratch. The offshore structure is a tripod made of steel tubes and piles with cones in the ends. The foundations meet the design requirements in shallow waters while being easy to install. This report is divided into Structural, Electrical, and Mechanical design. The interdisciplinary design approach left overlap among all the sections. We expect to generate enough electric power to charge a small electronic device, such as a smartphone.

1. Introduction

Juracan Energy Team (JET) worked during the assembly and testing phase to prover our weak points using our design idea. We analyzed the turbine structure to calculate the expected loads on the foundations. The testing of the foundations revealed that they could withstand the loads expected at the competition. The blades aerodynamics and hub rigidity were improved from the 2019 team design. The generator was designed, and the preliminary results are promising. However, the steel plates, coil manufacturing and coil fit within the stator could be improved. The control system needs further testing to ensure that the whole turbine will work as required by the competition deliverables.

2. Structural Design

2.1. Foundations Structural Analysis

The structure will experience loads due to gravity and wind pressure, since we are working on a small scale the effect of the forces of the waves was negligible. To determine the load capacity of each of the three piles, a full-scale structural analysis was performed in the RISA 2D program, taking into consideration the worst-case scenario which our tripod could experience. As seen in Figure 1, this is the most critical case when only one pile is acting in compression and only one in tension stabilizing the structure with the subjected loads and being able to obtain the reactions generated in the foundations.

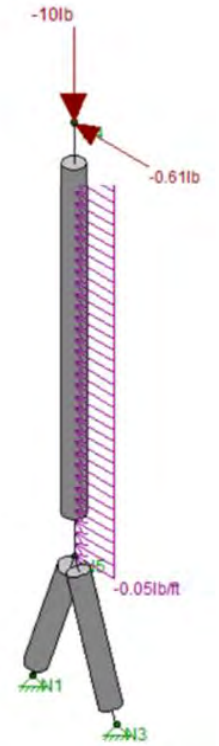

Figure 1. Forces applied to piles

Using the Load and Resistance Factor Design (LRFD) method we have applied loads of the tripod's own weight and that of the turbine as dead load (DL), which according to previous

models can approximate a joint weight of $10\ lb$. The wind loads (WL) on exposed structural components can be considered as a constant force therefore $F_w = (\rho\ /\ 2g)C_S A v^2$, where F_w is wing drag (lb), ρ is density of air (lb/ft^3), g is acceleration of gravity (ft/s^2), C_s is shape coefficient of long cylinder (0.82), A is area on plane (ft^2), and V is wind speed ($72.17 ft/s$). The load factor to be used in this case is $0.9DL\ + 1.3WL$ which implies that the structure will tend to fall over when reducing the weight and increasing the wind speed. The reactions obtained in the foundations are seen in Table 1.

Table 1. Node reactions

Node	Description	Reaction in X (lb)	Reaction in Y (lb)	Resulting Reaction (lb)	Moment Mz (Lb*ft)
N1	Pile in compression acts as pinned	4.883	31.25	31.629	0
N3	Pile in tension acts as pinned	1.901	-22.25	-22.331	0
Totals	-	6.784	9	9.298	0

2.2. Foundations Prototype Testing

Several 3D printed piles and a tripod that had been designed using SolidWorks were produced to be tested in the laboratory. The prototypes in Figure 2 helped us to compare the data obtained in the simulation assuming the worst-case scenario in which only one pile acts in compression and the other in tension. The forces tested were those that lift the structure and can cause it to overturn. The test was performed by first testing the vertical and lateral capacity of the single piles in dry sand and then in fully saturated sand (conditions of the competition rules). This was done using a spring scale and attaching it to the piles, then pulling until it lifted from the sand as can be seen in Figure 3.

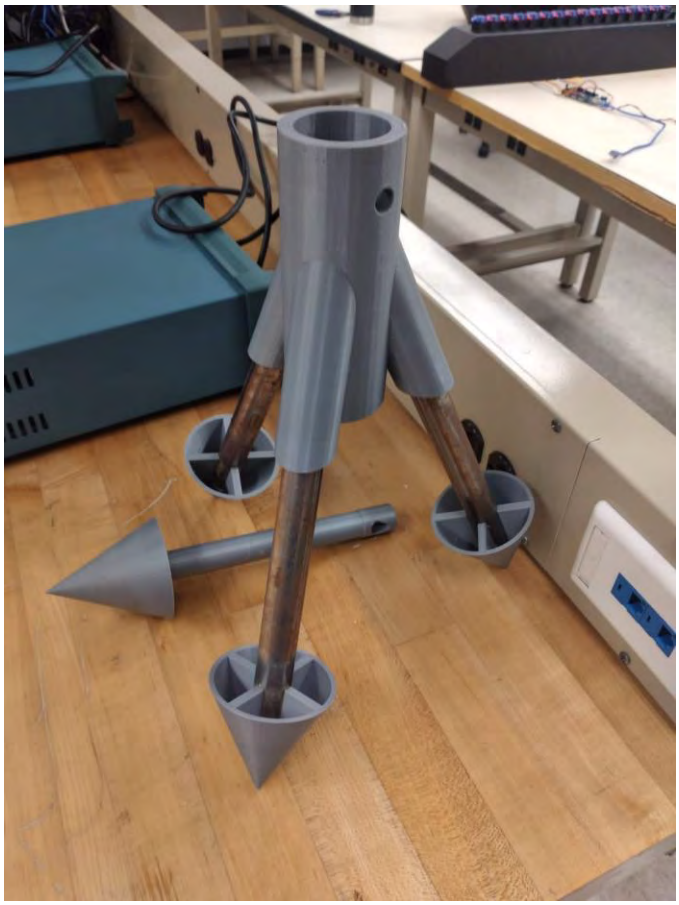

Figure 2. Foundation Tripod Assembly and Single Pile Below

Figure 3. Single pile at maximum resistance and after breaking loose

The resulting capacity in the simulation was $22.33\ lb$ and a result of approximately $23\ lb$ was obtained in the laboratory with a single pile. In the case of the tripod, it was tested without the turbine because the weight of the system would influence the results positively, counteracting the wind forces and established parameters. By having the tripod without weight, the capacity provided by the conical footing is observed. Under the conditions of the regulations, we placed the tripod in the sand with the water and confirmed that it can sink into the sand by vibrating the structure. The resulting experimental capacity generated by the tripod was up to a resistance of $30\ lb$ as can be seen in Table 2. Considering that all the simulations and tests were performed with the worst-case scenario in mind, the design for the structure should be able to manage the expected normal conditions with ease. Our testing was also done in a smaller tank, the additional sand in the competition setup will provide a better result as the sand activated by the cone will not be limited by the walls of our setup. This does not detract from the fact that there are areas for potential further improvements, particularly on the conical footing. Making the tip of the cones flatter could help the cones under stress sink less. Adjusting the height and diameter of the cone for better sand area coverage to provided additional weight and stability. Due to time constraints and removed requirement of foundations for learn-along teams we did not complete the cone and tripod fabrication from steel. The PLA parts were strong enough for testing purposes.

Table 2. Resistance test results

Test Attempt	Description	Resistance (lb)	Force Direction	Notes
1	Single pile just in sand	10	Vertical	Force was applied suddenly
2	Single pile in sand and water	23	Vertical	Force was applied gradually
3	Single pile in sand and water	12	Lateral	Force was applied gradually
4	Tripod in sand and water	15	Vertical	Force was applied gradually
5	Tripod in sand and water (Force directed at two piles)	23	Lateral	The hook on the spring weight hit the bucket, changed to an angle to prevent this.
6	Tripod in sand and water (Force directed at two piles)	25	45° Degree Angle	Force was applied gradually
7	Tripod in sand and water (Force directed at a single pile)	31	45° Degree Angle	Force was applied gradually

3. Electrical Design

3.1. Generator Design

To calculate the require number of turns we need the peak magnetic flux density at the coils during rotation. The AFPM is a 3D machine that requires complex and computing intensive Finite Element Method (FEM) magnetic analysis. For iterative design approaches this can become a bottleneck. For that reason, researchers have simplified the analysis by reducing it to a 2D model. This will provide an idea of how the design parameters affect the magnetic flux density inside the generator and can be extrapolated to a complete 3D FEM magnetic analysis. To simplify the analysis, we developed a FEA magnetic analysis using MATLAB and FEMM. FEMM provides the FEM toolkit and has a MATLAB Application Programming Interface (API) that can draw the geometry, select materials, run the simulations, and grad the results.

A way of reducing the dimensionality of the FEM analysis is the Linear Motor Model Approach (LMMA). Researchers in [2] proposed this method and show that the 2D-LMMA has the fastest solving times and is the most precise 2D method in their comparison. LMMA takes advantage of the symmetry of the machine and only uses one section at a constant radius. This section is seen as a 2D plane for the purposes of this analysis. The process of slicing and reducing dimensions can be appreciated in Figure 4.

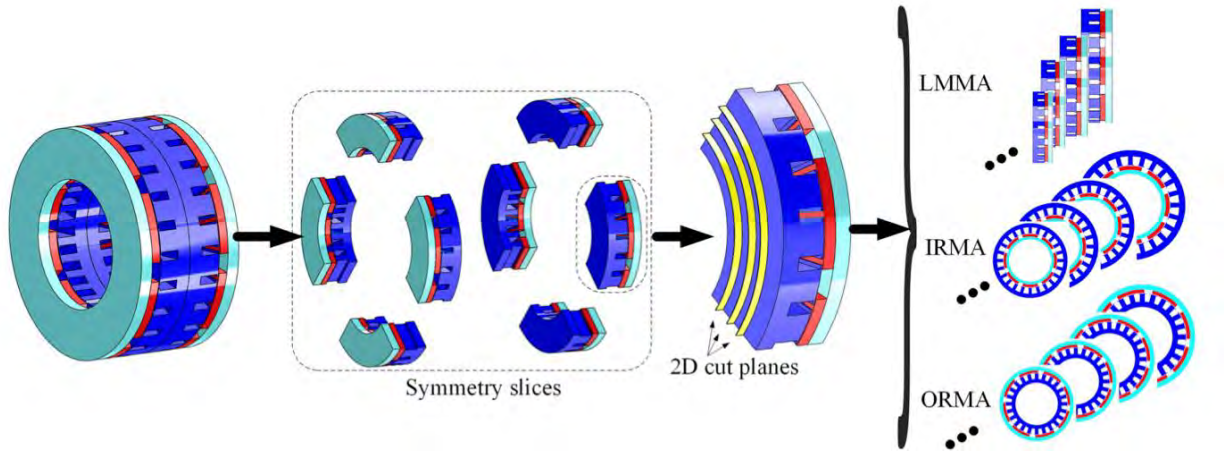

Figure 4. Reduction of 3D AFPM FEM Analysis to 2D FEM. Taken from [2]

Using the FEMM MATLAB API, we developed a MATLAB script. This has a series of design parameters that can be changed to alter the geometry, location of the magnets, number of magnets, materials, and dimensions. By using this approach of automating the drawing process we eliminate the time-consuming process of drawing all the parts each time a design parameter changes. The simulation output from FEMM using the script can be seen in Figure 5. The magnetic flux density at the middle of the generator, where the coils will be located, can be graphed using the simulation results. The Figure 6 shows the resulting magnetic flux density with respect to the horizontal position in 2D analysis. This position represents an angle in 3D analysis. We simulated a Halbach array, where the magnet polarity changes in intervals of 90º. We used 12 magnets to reduce the effects of the boundary conditions on the peak magnetic flux density. In addition, six coils were included to see how they behaved in the generator. The exported data shows a peak flux magnetic density of $B_{max} = 0.26184\ T$.

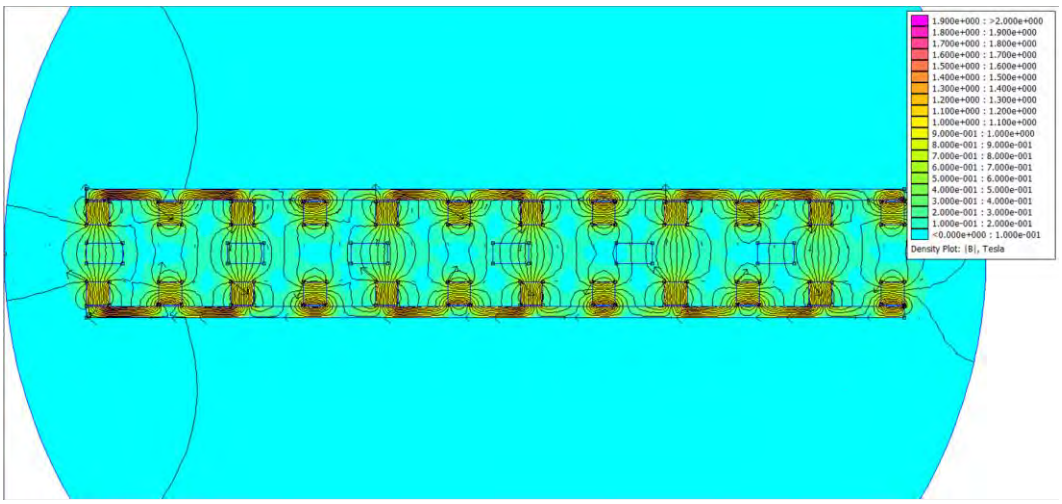

Figure 5. AFPM Generator Magnetic Finite Element Analysis with MATLAB/FEMM

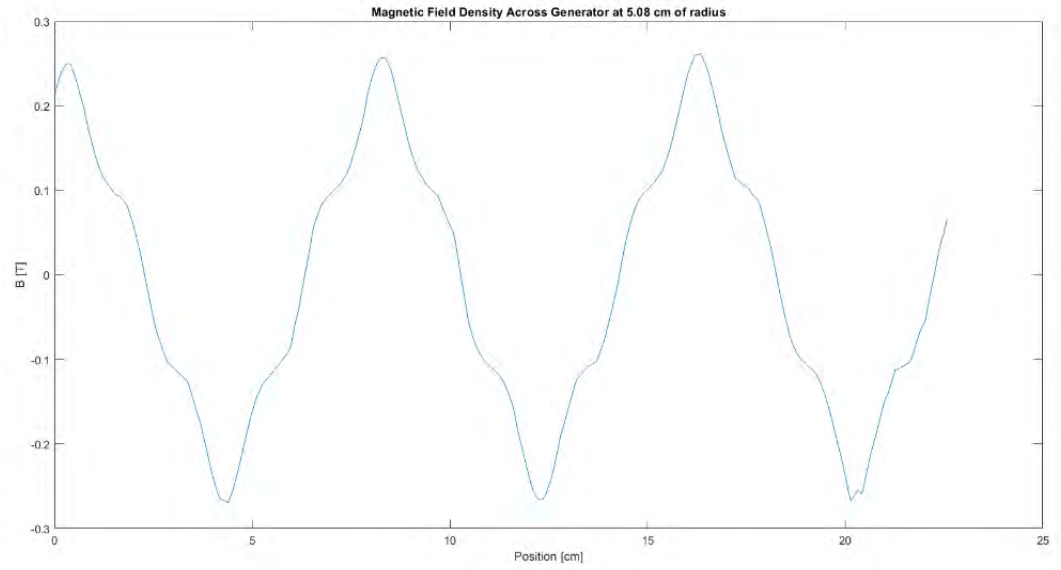

Figure 6. AFPM Generator Magnetic Field Density Across Coils

3.2. Electric Brake Testing

We are going to implement the electronic brake based on [1]. The circuit in Figure 7 works by charging the capacitor $C1$ and when the thyristor is triggered it lets $C2$ to charge up and activate $Q1$ that executes the braking. $Q2$ is the reset switch that discharges the capacitors and disables the electronic brake.

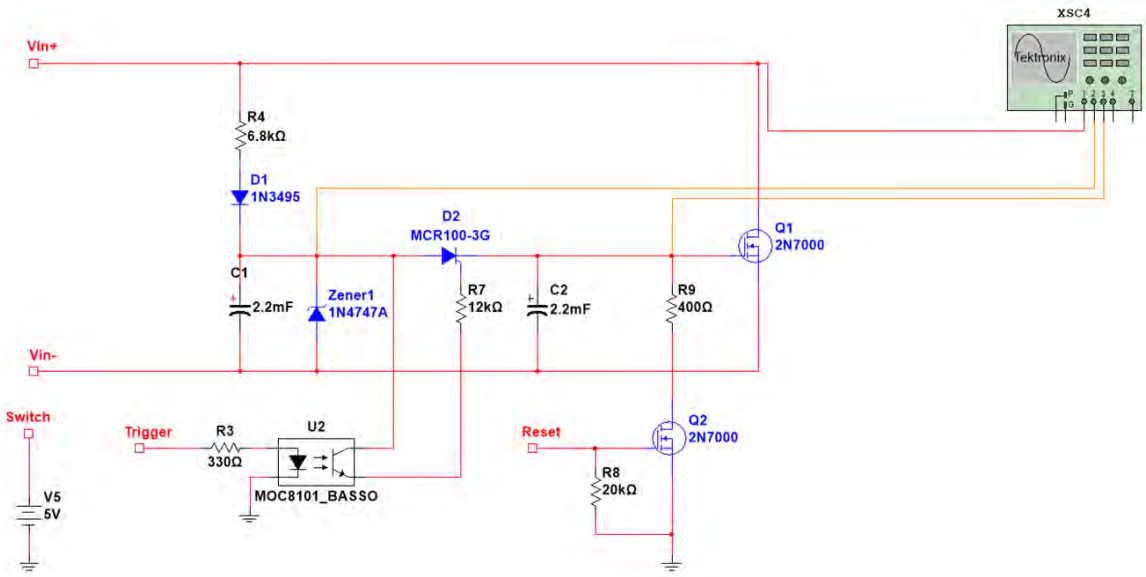

Figure 7. Electric Brake

To test the circuit, we used a power supply and multimeter. As seen in the DC power supply in Figure 8, once the Trigger pin is activated with 5V, the current will increase to $1\ A$ limited by the power supply caused by the MOSFET $Q1$. Hence, $Q1$ will begin to heat up, and slowing the wind turbine. When the Reset pin is activated, the current drawn from the turbine will decrease to $0\ A$ letting the turbine increase its speed.

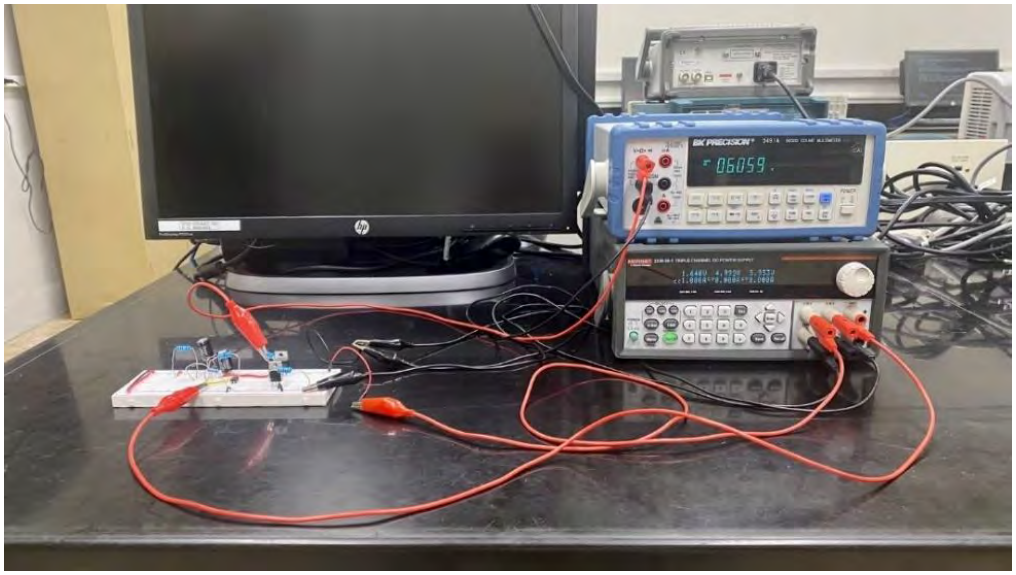

Figure 8. Electric Brake Test Set-Up

3.3. Generator Testing

The generator assembly in Figure 9 was tested by hand and using a drill. The rotational speed can be determined from as on a synchronous generator using Equation 1, where f is the frequency and p the number of poles, in our case 8 poles. In Figure 10, we reached 27 V_{pk-pk} for a rotational speed of $1{,}300\ RPM$ at open circuit. Attaching a load of $10\ \Omega$ at this speed, it

consumed $11W$ of power. Further testing needs to be done to complete the power curve of the generator. More details on the mechanical design are provided in Section 4.3.

$$n_m = \frac{120f}{p} \quad (1)$$

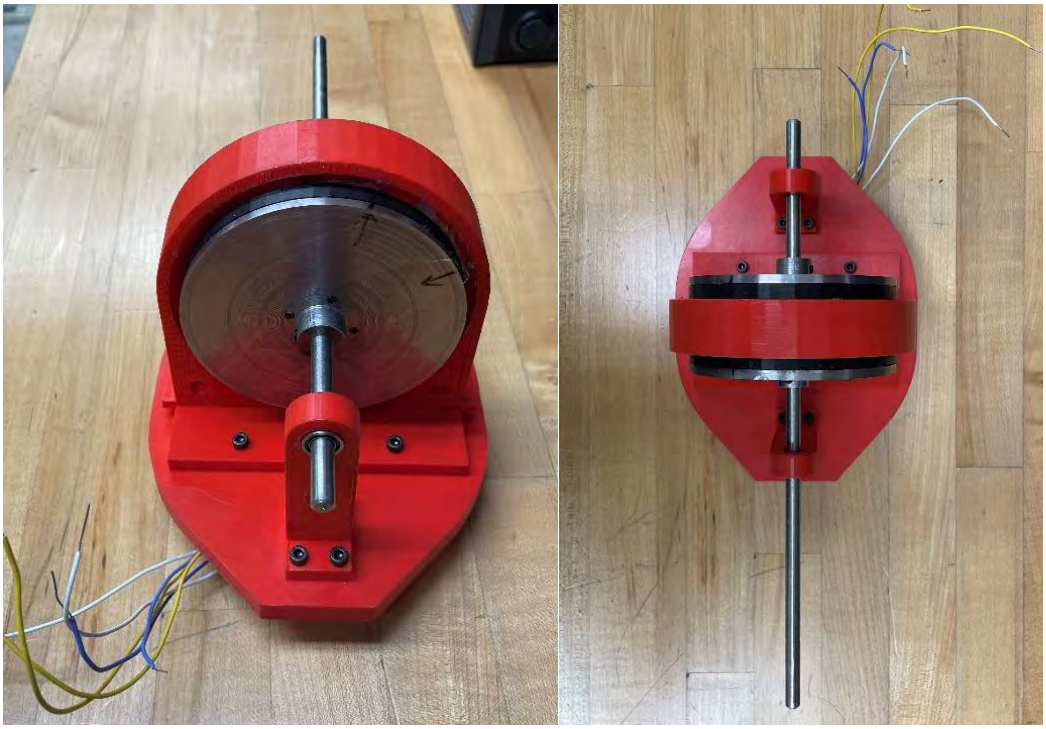

Figure 9. Generator Final Assembly

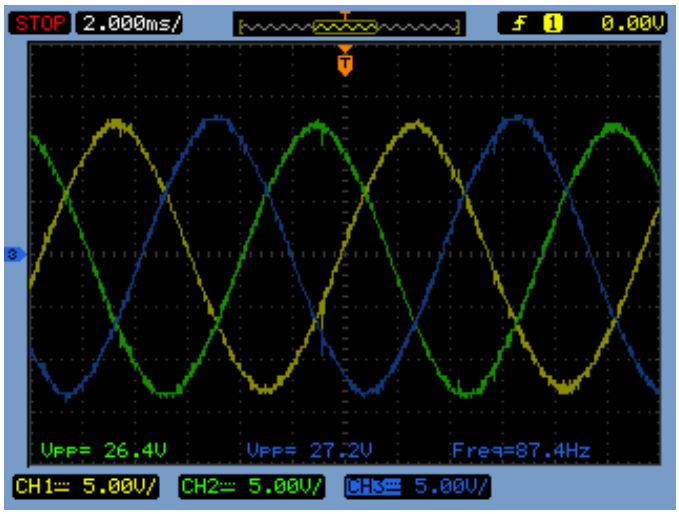

Figure 10. Open Circuit Generator Induced Voltage at 1,300 RPM

3.4. Control Circuit

The control system for the turbine will collect data from input and output voltage, input and output current, and emergency stop button to take decisions on the turbine operational

state. Figure 11 shows the connections for the control system. The signals will be collected by an Arduino microcontroller and the data will be periodically sent via serial communication to a SparkFun Qwiic OpenLog module.

The Figure 12 shows the final build for the control box. The same components and connections seen in the block diagram are found in the physical control box. The bottom left corner includes the connection to the generator and the three-phase rectifier. The top left corner includes the buck-boost converter and the electric brake on a protoboard. In the bottom middle portion of the box, the Arduino microcontroller can be seen. On the right side of the box the voltage and current sensor filters are mounted on a breadboard followed by the PCC connections on the top right. Finally, on the outer right side of the control box, it showcases the emergency stop button, the external power supply input, and the load connection. We would be using a benchtop electronic load for this purpose.

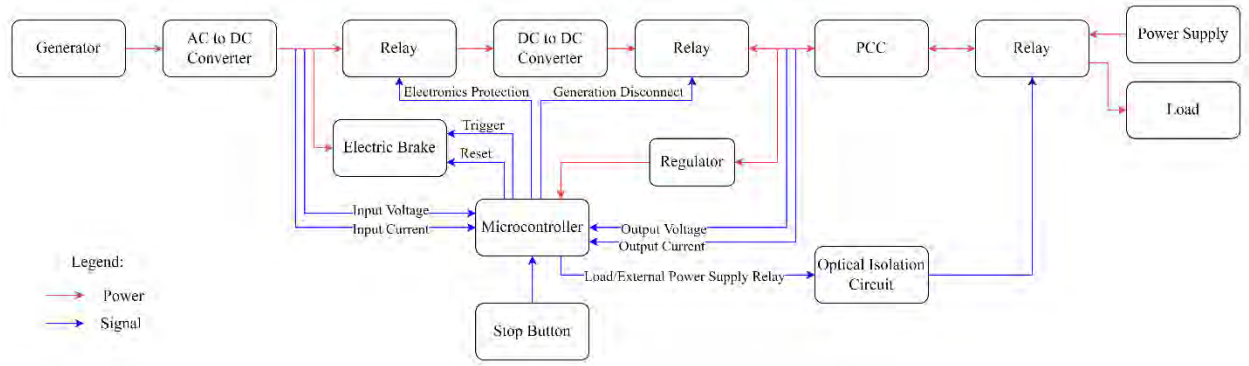

Figure 11. Block Diagram

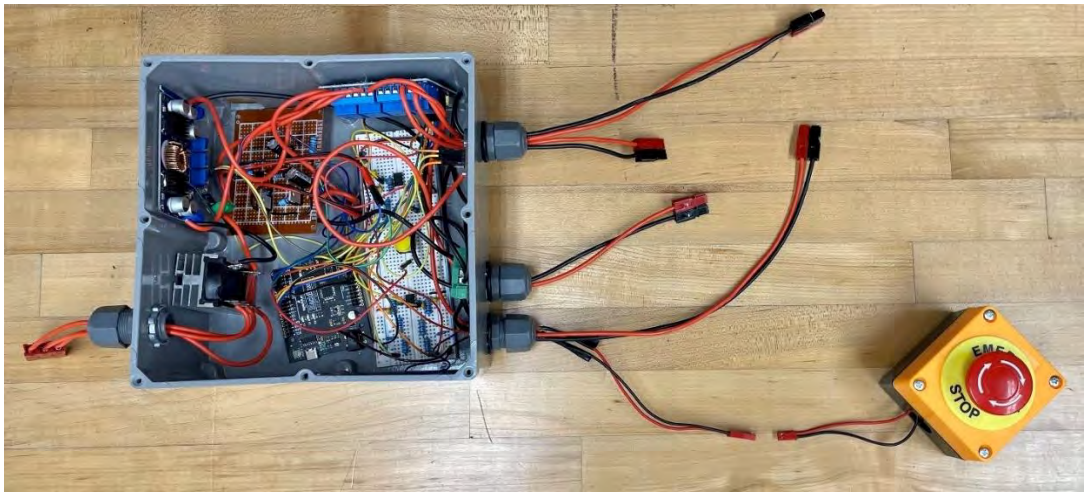

Figure 12. Control Circuit Box

The Figure 13 shows the main control logic for the turbine. The voltage and current functions read and calculate the input and output voltage and current respectively. They are stored in global variables. Based on the initial readings, and the current operational and brake state, the turbine decides if it continues on the OFF or generating state. Then it decides if braking is needed and executes a procedure to store the current operational states to the EEPROM

memory, switch the relays simultaneously using port register control, and then triggers the braking circuit. The program doesn't have delays and runs continuously. To avoid overwhelming the user with data we implemented a timed procedure to log the data in a Comma Separated Value (CSV) format only after the refresh interval is completed. The data can be read from a computer with the USB port for troubleshooting or with the SparkFun Quiic OpenLog module to save the data in an SD card while the turbine is running to be analyzed after testing.

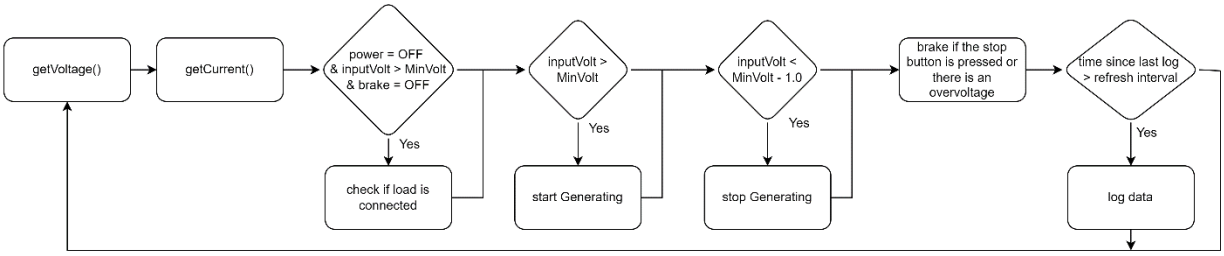

Figure 13. Control Logic Loop

3.5. Voltage and Current Sensor Filters Testing

The filters for the voltage and current sensors were tested with a function generator and oscilloscope. On the oscilloscope readings, the green represents the output signal and the yellow represents the input signals. Observe at Figure 14 the voltage gain of 1 at $500Hz$, demonstrating a pass band behavior. Figure 15 shows the signals at $1.1kHz$, with a gain of 0.73, about $-3dB$ marking the cutoff frequency.

Figure 16 shows the signals at $5kHz$, the signal shows a voltage gain of 0.448, below the 0.707 gain at cutoff demonstrating a stop band behavior. Each filter was tested and got similar results with differences that can be attributed to component tolerances.

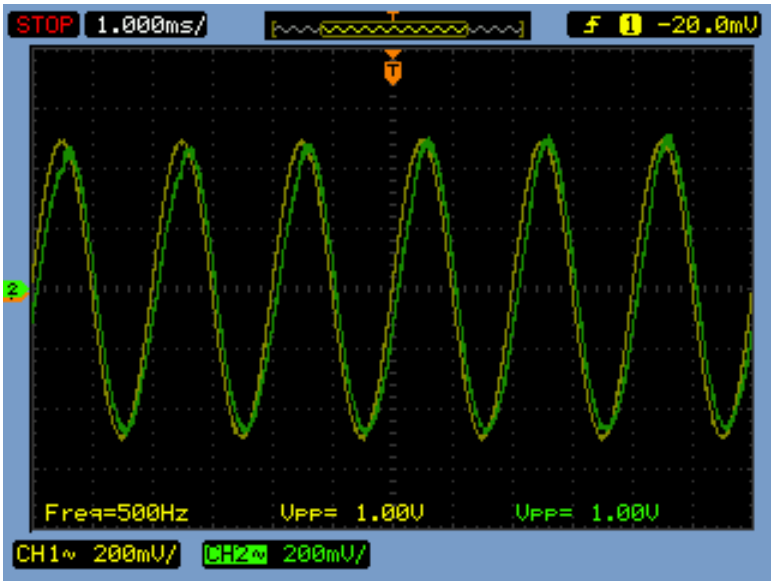

Figure 14. Pass Band Gain

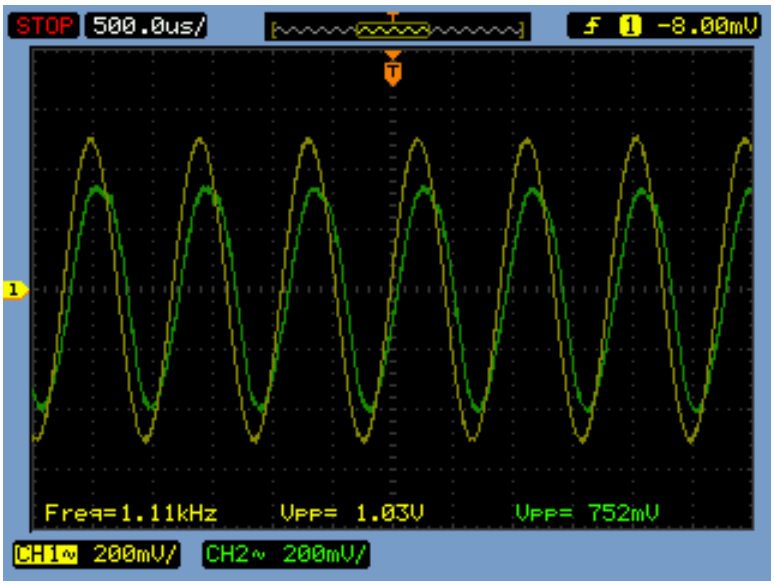

Figure 15. Cut-Off Frequency Gain

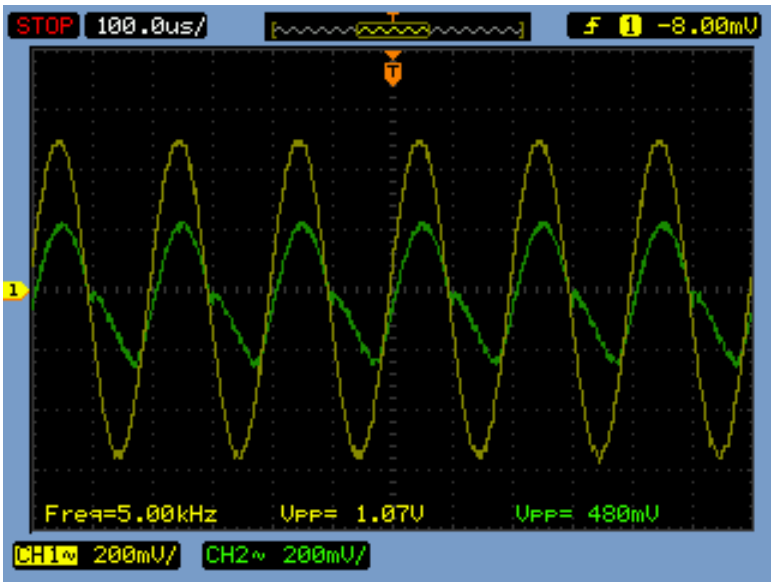

Figure 16. Stop Band Gain

4. Mechanical Design

4.1. Blades

Using the same S1223 airfoil from the 2019 turbine, the team optimized the chord and twist of the blade sections using the ideal rotor with and without wake rotation models from [2] with Excel. A Python script was used to export the blade sections with the proper chord and twist from the Excel results to accelerate the CAD modeling process. The team members used QBlade to simulate the blade and get the power curves in Figure 17. The new blade designs have a lower peak C_p but is a quicker and more sustained response. We plan to test both blade models using different testing spots to compare their performance in practice.

Figure 17. Blades Coefficient of Power Curve

4.2. Hub

In our 2019 design, the hub design had a stress concentration point between the blade connectors. The screws and little clearance created a 3D print file that left a gap on the connector joints leading to a catastrophic failure when the turbine was tested in the competition. To address this issue, the connector and hub was redesigned to leave more material between the connectors and the hub screws. The Figure 18 shows the hub model, to improve the thread durability we used metal inserts that were pressed with heat into the front section of the hub. This will avoid excessive wear on a plastic thread and enhance the strength of the area. A clevis pin will be used to attach the hub to the shaft and will be locked in place with a cotter hairpin. The rotor assembly was tested on a milling machine to simulate the high rotational speed that it could experience in the competition. The hub presented no issue running up to $2{,}750\ RPM$. The design uses three screws to hold the blades permitting quick blade changing in case of failure.

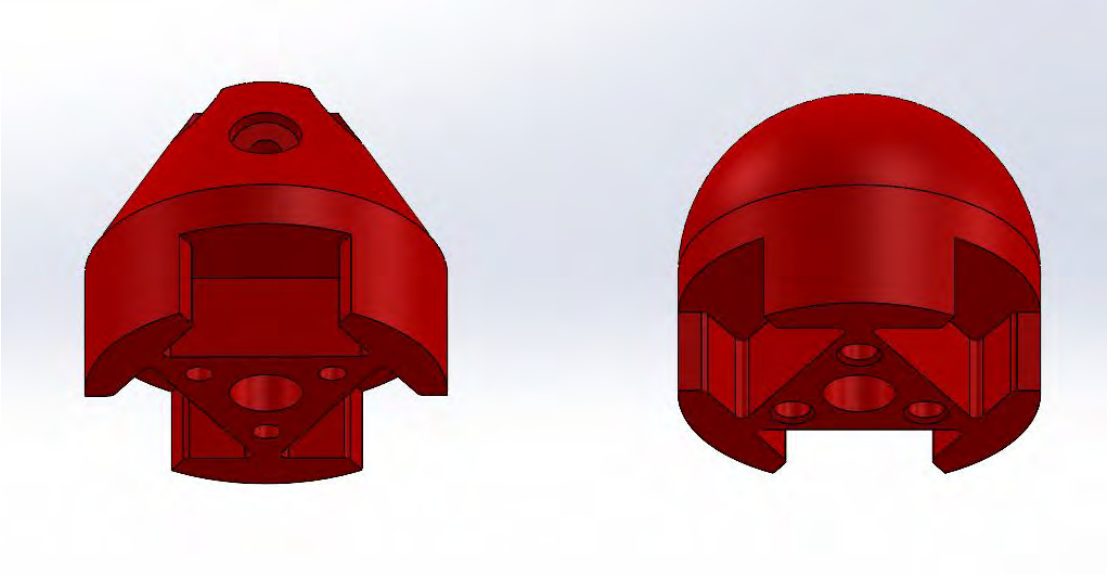

Figure 18. Hub Features (Back on the left, Front on the right).

4.3. Generator

An Axial-Flux Permanent Magnet generator topology was chosen as it is easy to manufacture and efficient. Two parallel rotors made of 1018 steel and 3D printed PLA magnet aligners. Each rotor used 16 N52 magnets of 0.25” by 0.25” by 1.0” were placed in Halbach arrays and the rotors were positioned with opposing polarity on the shaft. Those design choices were made to maximize the magnetic flux in the center of the generator. The steel rotors were manufactured on the lathe and fixed with set screws on the shaft. The hardest part of manufacturing the steel plates is to align them correctly to avoid uneven machining that could induce vibrations at high speeds. The magnet alignment plates were 3D printed and screwed to the steel plates with 4 screws on the front. The stator was 3D printed with PLA and the coils were manufactured using an in-house made coil winder. From our calculations, we determine that each coil needed 220 turns of 24AWG wire to fit in the stator and generate the amount of power that we wanted. The stator is swappable to ease the manufacturing and troubleshooting. The CAD model can be seen in Figure 19 and the stator can be seen in Figure 20.

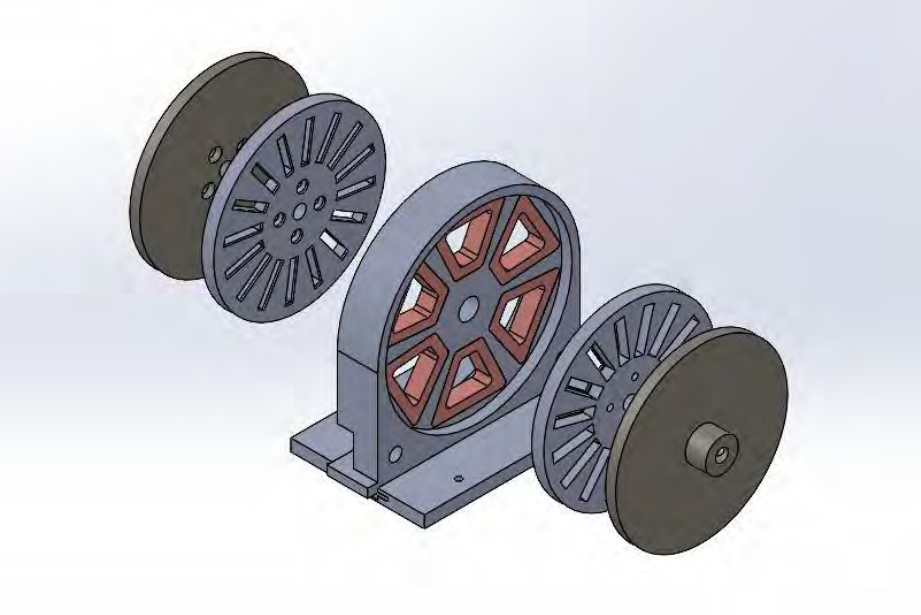

Figure 19. Generator CAD Model

Figure 20. Generator Stator Assembly

4.4. Nacelle, Turntable, and Tail

Using the same tower and base flange from the 2019 design, the nacelle was redesigned to fit the generator. At first the nacelle was originally going to be one part but during the process we figured that it was difficult remove to exchange inner components. The biggest challenge of the nacelle was to design a shell that can cover the generator with a good airflow. Looking at the older design we came to the decision to simplify the cover removal process. The team determined that a two-piece nacelle as seen in Figure 21 was the best approach to simplify the

removal. The sections of the nacelle are supported with the generator and fixed with screws from the back to the front section. The flow simulation in Figure 22 ensured that the airflow of the blade was not interrupted from the aerodyanmics of the Nacelle. The turntable consists of a 1” bearing with its corresponding supports below the nacelle and on the tower. The bearing will be press fited in the supports and those will be secured in place with screws. The tail design was a simple wind with the team logo on the side. It will be held in place with a shaft and set screw. The prototype assembly can be seen in Figure 23. The shaft is supported by four bearings, two on outer supports and two in the generator stator.

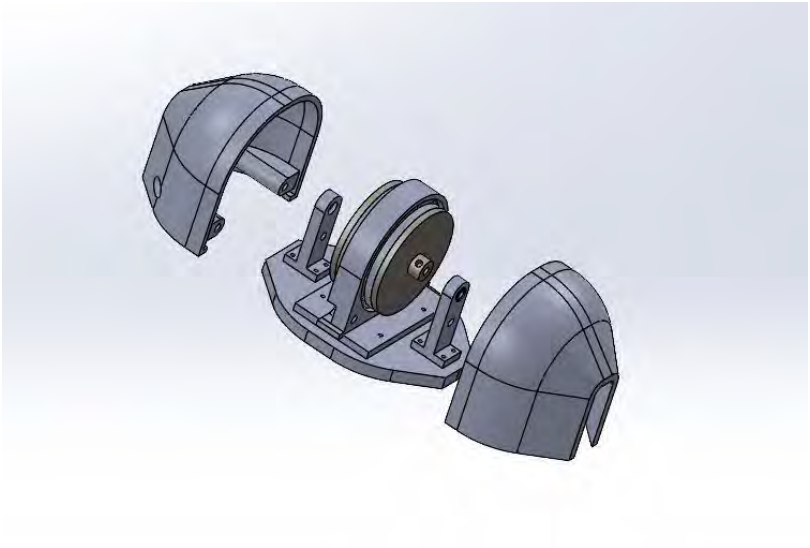

Figure 21. Nacelle Exploded View

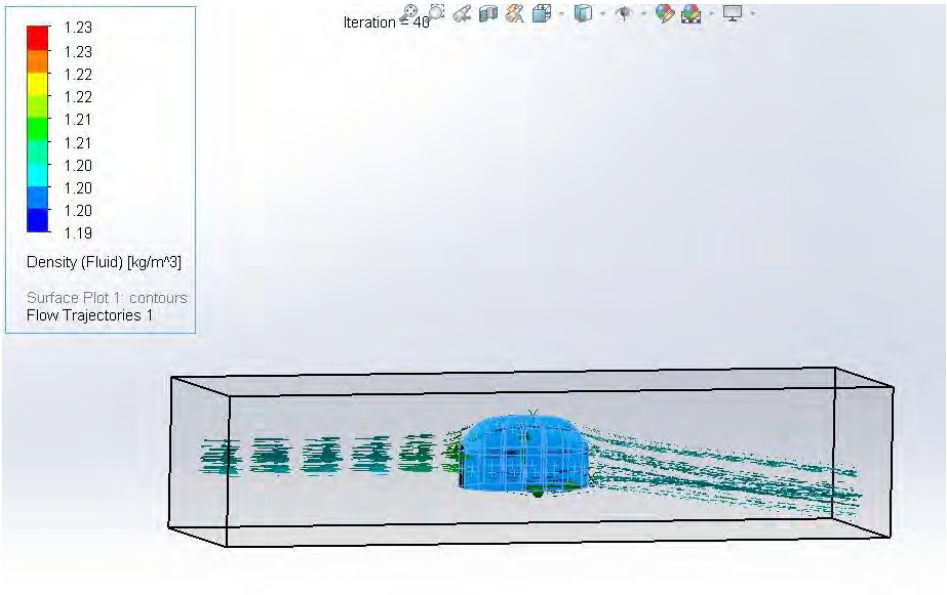

Figure 22. Air Flow Simulation on the Nacelle

Figure 23. Turbine Assembly

5. Turbine Assembly Checklist

To start the final assembling the first step was unify the lower part of the turntable with six M6 Allen Screw and 1” Ball Bering to the nacelle base. Then, the bearing is pressed onto the turntable hub. We attach the shaft brackets with four M4 Allen screws and insert a 0.5” Stainless Steel Ball Bearings onto them. This goes the generator stator that is going to be inserted into its sliding base and screwed in place with four M4 Allen screws. Next the shaft is introduced in the shaft bracket to align with the generator but first the first magnet alignment and magnet cover are added that will go to 0.5cm of the generator to then do the same procedure but on the rear side of the turbine. After aligning the shaft with all the components for the generator, the tail goes with its own shaft in the rear bracket of the turntable. With that we install the Nacelle, first introduce the rear Nacelle with the generator that has two 0.38” holes that align the Nacelle afterward the front Nacelle goes align with the same holes that the generator and the rear Nacelle have. Finally, we installed the tower through the lower hub.

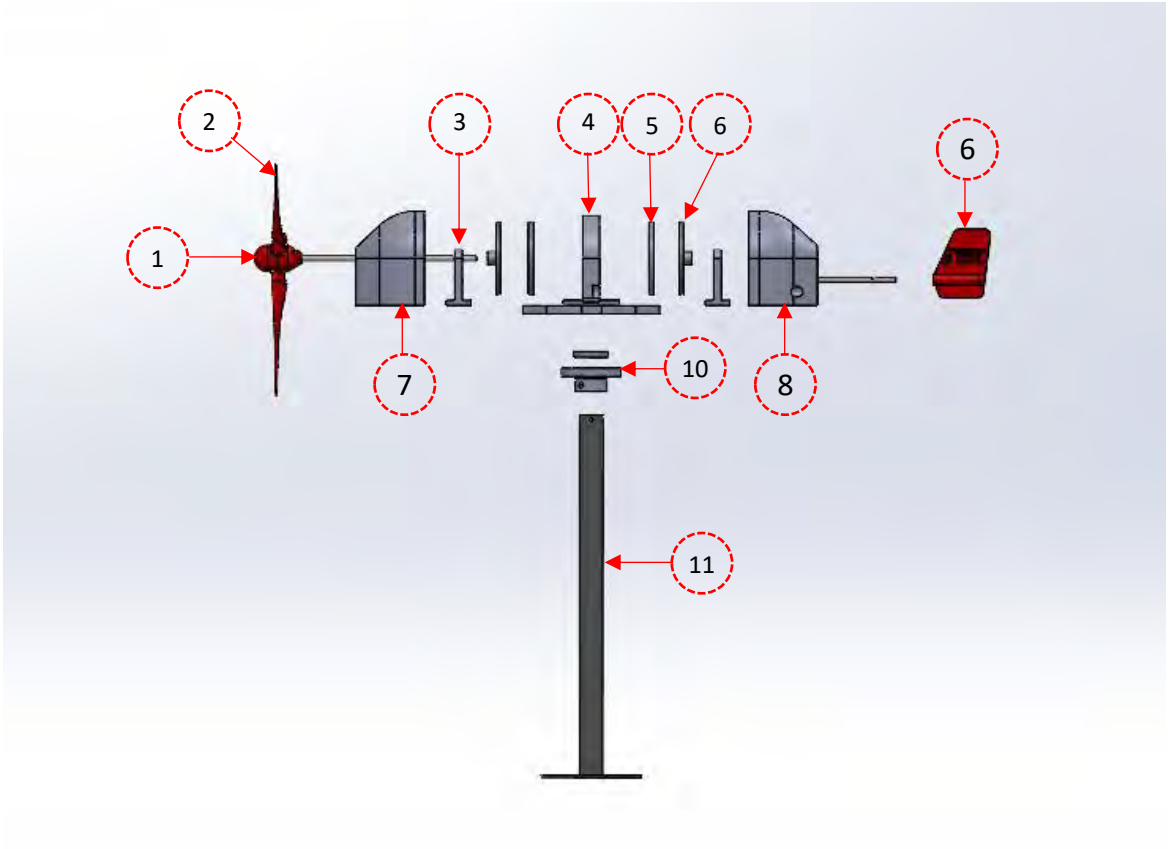

Figure 24. Turbine Exploded View

Table 3. Turbine Components from Exploded View

Part Number	Description
1	Hub
2	Blades
3	Shaft Support Tower
4	Generator Stator
5	Generator Rotor Magnet Alignment
6	Generator Rotor Steel Backplate
7	Tail
8	Front Nacelle Case
9	Back Nacelle Case
10	Turntable
11	Tower

6. Conclusion

The team developed new design approaches for the blades and generator. We began the design validation process where we can see that the turbine will have a low cut-in wind speed. There is more testing needed for the control system before the competition. However, the generation tests show promising results.

7. References

[1] G. M. Hiraldo-Martínez, A. D. Santiago-Vargas, D. A. Aponte-Roa and M. A. Goenaga-Jiménez, "Automatic Electronic Braking System for Commercial Micro Wind Turbine," in *ASME 2021 Power Conference*, Virtual, Online, 2021.

[2] J. G. M. A. L. R. J. F. Manwell, Wind Energy Explained: Theory, Design and Application, John Wiley & Sons, Ltd, 2009.

[3] D. C. Meeker, "Finite Element Method Magnetics," 28 February 2018. [Online]. Available: https://www.femm.info/.

[4] M. Gulec and M. Aydin, "Implementation of different 2D finite element modelling approaches in axial flux permanent magnet disc machines," in *IET Electric Power Applications*, 2017.